

Enhancing Physical Layer Security in LEO Satellite-Enabled IoT Network Communications

Anna Talgat, *Student Member, IEEE*, Ruibo Wang,

Mustafa A. Kishk, *Member, IEEE*, and Mohamed-Slim Alouini, *Fellow, IEEE*

Abstract

The extensive deployment of Low Earth Orbit (LEO) satellites introduces significant security challenges for communication security issues in Internet of Things (IoT) networks. With the rising number of satellites potentially acting as eavesdroppers, integrating Physical Layer Security (PLS) into satellite communications has become increasingly critical. However, these studies are facing challenges such as dealing with dynamic topology difficulties, limitations in interference analysis, and the high complexity of performance evaluation. To address these challenges, for the first time, we investigate PLS strategies in satellite communications using the Stochastic Geometry (SG) analytical framework. We consider the uplink communication scenario in an LEO-enabled IoT network, where multi-tier satellites from different operators respectively serve as legitimate receivers and eavesdroppers. In this scenario, we derive low-complexity analytical expressions for the security performance metrics, namely availability probability, successful communication probability, and secure communication probability. By introducing the power allocation parameters, we incorporate the Artificial Noise (AN) technique, which is an important PLS strategy, into this analytical framework and evaluate the gains it brings to secure transmission. In addition to the AN technique, we also analyze the impact of constellation configuration, physical layer parameters, and network layer parameters on the aforementioned metrics.

Index Terms

Physical layer security, stochastic geometry, LEO satellite-based IoT network, artificial noise techniques, uplink transmission.

Anna Talgat, Ruibo Wang, and Mohamed-Slim Alouini are with KAUST, CEMSE division, Thuwal 23955-6900, Saudi Arabia. Mustafa Kishk is with the Department of Electronic Engineering, Maynooth University, W23 F2H6, Ireland. (e-mail: anna.talgat@kaust.edu.sa; ruibo.wang@kaust.edu.sa; mustafa.kishk@mu.ie; slim.alouini@kaust.edu.sa. Corresponding author: Ruibo Wang.)

I. INTRODUCTION

A. Motivation

Low Earth Orbit (LEO) satellites play a crucial role in enhancing the connectivity of the Internet of Things (IoT) devices, especially in remote and underserved areas where traditional terrestrial networks struggle to provide coverage [1]–[3]. The rapid expansion of satellite launches, which has been growing by 30% annually since 2012, is due to advancements in rocket launch platforms [4]. This brings enormous opportunities for the connectivity of IoT devices but also poses new challenges for communication security.

The deployment of mega-constellations makes more satellites act as potential eavesdropping threats, especially for uplink transmission from IoT devices to satellites. Furthermore, due to the dynamic nature and high speed of LEO satellite constellations relative to the Earth, there are frequent changes in the signal quality received by both the primary and potential eavesdropping channels. Atmospheric conditions, multipath fading, and interference further impact the signal. At certain times, the main channel may experience poor conditions, resulting in a weaker received signal. Simultaneously, an eavesdropper may be in a location with better channel conditions, leading to it experiencing a stronger signal. For example, rain fade can weaken the main channel signal, while an eavesdropper in a clear sky region may experience less attenuation and, therefore, better signal quality. This variability can lead to scenarios where the eavesdropper receives a higher quality signal than the main communication link, thus posing a significant security threat. Therefore, the urgent need for enhancing uplink security strategies should be emphasized.

To address these challenges, our research integrates the Stochastic Geometry (SG) analytical framework with advanced Physical Layer Security (PLS) techniques. This novel combination enables comprehensive analysis of dynamic topology and interference, providing low-complexity solutions for evaluating security performance in IoT networks based on multi-tier LEO satellite constellations.

B. PLS Techniques in Satellite Networks

Recently, PLS techniques have been increasingly recognized as potential solutions for enhancing security within satellite networks. The idea of PLS originates from Shannon’s foundational concept about perfect secrecy. Subsequently, authors in [5] proposed the eavesdropper channel model, considering that the information received by the eavesdropper is a degraded version of the legitimate received information.

The core idea of applying PLS in satellite networks is to use the randomness of wireless channels, such as interference, fading, and noise, to achieve secure transmission [6]–[9]. A notable example is the Artificial Noise (AN) technique, which was first proposed in [10]. The principle of AN technology is that the IoT device generates an additional interference signal while transmitting useful signals [11]. This interference signal can be filtered out by legitimate receiving satellites during demodulation, thereby affecting only the eavesdropping satellites [12]. As a result, IoT devices reduce the signal quality of the eavesdropping link by sacrificing some of their own power to transmit AN.

Several pioneering studies have advanced the integration of PLS techniques within satellite communications. Authors in [13] provided foundational frameworks by optimizing resources for secure satellite communications across different receiver scenarios, including fixed and mobile units, while [14] provided a detailed theoretical analysis on securing non-geostationary orbit satellite downlinks. Further, research like [15] introduced threshold-based user scheduling to improve secrecy in multiuser systems, and [16] proposed cooperative secrecy tactics in LEO-integrated networks through jamming signals and optimized power allocation. Moreover, [17] explored the role of unmanned aerial vehicles (UAV)s in strengthening satellite-vehicular communication security, and [18] leveraged time-packing techniques to safeguard IoT devices' direct satellite links. Additionally, recent advancements in PLS techniques include secrecy-energy efficient hybrid beamforming for satellite-terrestrial integrated networks to improve security and energy efficiency [19], signal-to-leakage-plus-noise ratio (SLNR)-based secure energy-efficient beamforming applied in multibeam satellite systems [20], and refracting reconfigurable intelligent surface (RIS)-aided hybrid satellite-terrestrial relay networks developed for joint beamforming design and optimization [21]. Furthermore, rate-splitting multiple access, which indirectly supports PLS by improving interference management and signal reliability, has been used to support IoT in satellite and aerial-integrated networks [22]. These studies demonstrate the wide range of PLS applications in safeguarding satellite communications against potential security threats, highlighting the most recent developments in improving the security and efficiency of satellite and IoT networks.

Although the issue of PLS has gained wide attention in the field of satellite communications, there are still some challenges that remain unresolved. The first challenge is that the satellite network's topology is dynamic; thus, the number of eavesdropping and legitimate satellites follow a specific stochastic distribution. Furthermore, the spatial distribution of satellites also greatly

influences the probability of eavesdropping or successful transmission [23]. The second challenge is that the deployment of a large number of devices makes the interference hard to ignore [24]. Finally, as the number of satellites and IoT devices increases, evaluating the effectiveness of PLS strategies becomes increasingly challenging. This is because more device locations need to be generated, and more IoT-satellite links need to be simulated [13], [16]. Therefore, the third challenge lies in evaluating the performance of PLS strategies with low computational complexity.

C. Related Works for Stochastic Geometry

SG is a mathematical tool that can perfectly address the above challenges. It is one of the most suitable methods for analyzing large-scale random network topologies [25], and the SG-based analytical framework can account for stochastic variations in interference [26]. The analytical expressions derived within the SG framework can be represented as functions of system parameters such as the number of satellites [27]. Therefore, we can achieve a low-complexity mapping from system parameters to performance metrics, and the complexity does not increase with the scale of the constellation [28]. Next, we will introduce the research related to satellites and PLS in the field of SG.

Modeling satellites through the SG model is an emerging research method. Binomial Point Process (BPP) is one of the most widely used satellite modeling methods [29], [30]. The topological performance (such as the distribution of distances between communication parties [31]) and the network-level performance (such as coverage probability and data rate [32], [33]), derived from BPP, align well with actual satellite constellation outcomes. Compared to BPP, Poisson Point Process (PPP) is more suitable for modeling networks in non-closed areas [34], [35], such as ground-based IoT networks. Among SG-based satellite works, studies most closely related to our paper are [36], [37] and our previous work [38]. Our past research [38] involved addressing coverage issues in multi-tier satellite networks, where contact distance and association strategies laid the groundwork for this paper. However, [38] did not involve IoT devices or PLS issues. While [36] studied PLS in the downlink LEO satellite networks, focusing on the spatial distribution of satellites, users, and potential eavesdroppers modeled using homogeneous spherical PPP with eavesdroppers located on the ground. As for [37], authors explored the effect of single-tier satellite eavesdroppers on uplink transmission. The study provided support and inspiration for the research scenario of this paper. Unlike our paper, however, authors in [37] did

not consider PLS techniques, nor did it involve modeling of legitimate constellations. Therefore, our study significantly extends the scope beyond [37].

Additionally, some literature has utilized the SG framework to analyze the secure communication performance of planar networks [39], [40]. Authors in [41] initiated PLS methodology within cellular networks, and authors in [42] further explored this concept within millimeter-wave relaying networks. Authors in [40] expanded the SG framework to IoT networks, where sensors, access points, and eavesdroppers are modeled by PPPs. Furthermore, authors in [11] and [43] introduced AN technique into secure transmission in terrestrial networks, highlighting the significance of utilizing spatial randomness and strategic AN allocation. Although these studies have laid a solid foundation for researching PLS strategies in the SG field within ground networks, investigating PLS issues in satellite networks still faces many challenges. The spherical topology, channel models, and performance metrics, such as availability in satellite networks, are significantly different from those in ground networks.

D. Contribution

As the first study for PLS in satellite networks under SG, the specific contributions are as follows:

- We introduce a novel multi-tier satellite network topology for uplink transmission, where one tier consists of legitimate satellites while other tiers consist of potential eavesdroppers. This topology, which includes satellites at various altitudes serving distinct roles, accurately reflects the complexity of real-world LEO satellite constellations.
- We develop an analytical framework using SG to model the spatial distribution and interaction of satellites and IoT devices. This framework allows us to derive low-complexity analytical expressions for key performance metrics: satellite availability probability, coverage probability, secrecy outage probability, successful communication probability, and secure communication probability.
- By incorporating the AN technique within our SG-based analytical framework, we enhance physical layer security. This technique, with the strategic allocation of power to AN, degrades the signal quality perceived by potential eavesdroppers while maintaining the communication quality for legitimate receivers, thereby improving secure transmission performance.

- We conduct Monte Carlo simulations to validate the accuracy of our analytical results. These simulations confirm that the derived expressions can serve as accurate and low-complexity alternatives to more computationally intensive simulations for performance evaluation.
- We reveal useful system-level insights regarding the impact of constellation configuration (such as the number of satellites and their altitude), physical layer parameters (such as beamwidth), and network layer parameters (such as IoT device density) on availability probability and secure communication probability. These insights offer practical guidelines for optimizing secure LEO satellite-enabled IoT networks.

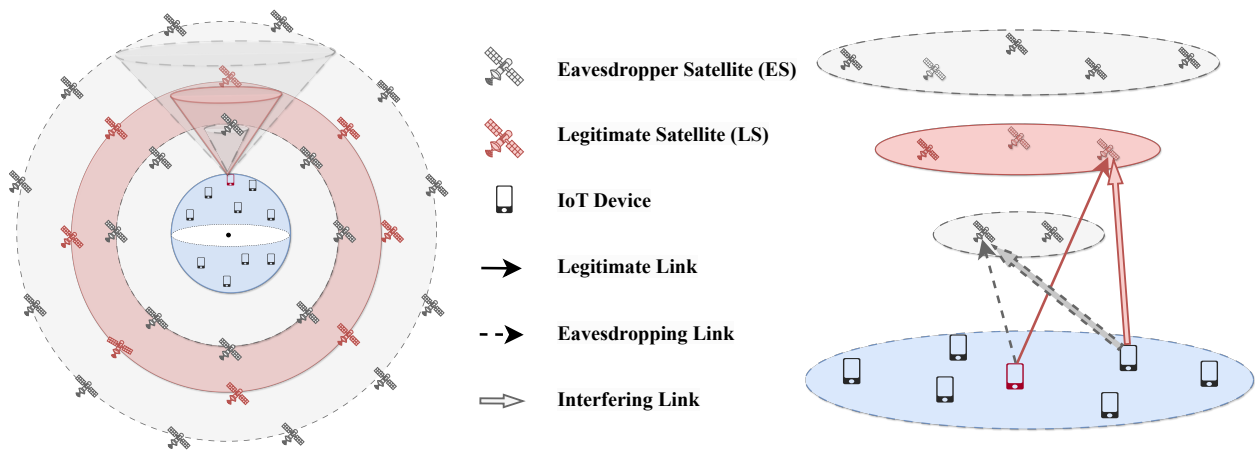


Fig. 1: Illustration of the multi-tier architecture of the network, depicting LS and ES at various altitudes. This configuration enables detailed analysis of signal interactions and security measures across different altitude levels.

II. SYSTEM MODEL

This section presents the system model for our investigation into enhancing the security of IoT communications through LEO satellites using PLS techniques. We consider uplink transmission in a multi-tier LEO satellite network with terrestrial IoT devices. In addition, we employ AN as a countermeasure against potential eavesdropping threats. The symbols, key abbreviations, and their meanings are listed in TABLE I.

A. Spatial Distribution Model

The IoT devices are distributed across the Earth's surface, following a homogeneous PPP model, which closely reflects real-world conditions. The PPP is denoted as $\Phi_u \equiv \{\mathbf{u}_i\} \in \mathbb{R}^3$ with density λ_u . IoT devices transmit their data to the designated LEO satellites. Without loss of

generality, the typical IoT device is assumed to be located at $\mathbf{u}_0 = (0, 0, R_\oplus)$ in the spherical system, where the R_\oplus is the radius of the Earth (≈ 6371 km). Apart from the typical device, other IoT devices act as potential sources of interference in the uplink transmission.

We consider a K -tier LEO satellite constellation with different altitudes a_k , where $k = 1, \dots, K$. Satellites from the k -th tier follow a homogeneous BPP on the surface of a sphere S_k with radius $R_k = a_k + R_\oplus$, where the positions of N_k satellites in the k -th tier are independent, identically distributed (i.i.d.). The sphere S_k can be expressed with spherical coordinates as $S_k = \{R_k, 0 \leq \theta \leq \pi, 0 \leq \varphi \leq 2\pi\}$, where θ and φ are polar angle and azimuthal angle, respectively. Finally, we denote the location of satellites on k -th sphere, as $\Phi_{S_k} \equiv \{\mathbf{x}_{kj}\}$ where $\mathbf{x}_{kj} \in \mathbb{R}^3$ indicates the location of j -th satellite on k -th tier. As shown in Fig. 1, the satellites in the constellation serving the IoT devices are legitimate satellite (LS)s, while other satellites potentially intercepting communications from IoT devices are known as eavesdropper satellite (ES)s. The K -tier LEO satellite constellation includes a legitimate tier composed of LSs, as well as $K - 1$ tiers consisting of ESs.

The multi-tier architecture, as illustrated in Fig. 1, represents a realistic deployment scenario where satellites are positioned at varying altitudes. This structure allows for an in-depth analysis of signal propagation and interception across different layers, enhancing the practical relevance of our study. By considering satellites at multiple altitudes, we can evaluate complex interaction dynamics and develop more effective PLS strategies.

B. Channel Model

In our channel model, we combine the effects of large-scale and small-scale fading to represent signal propagation accurately. The large-scale fading component, modeled by the free-space path loss, accounts for the overall signal attenuation due to the distance between the transmitter and the receiver. This component is expressed as $\left(\frac{c}{4\pi f_c d_{k,j,i}}\right)^2$, where f_c indicates the carrier frequency, c is the speed of light and $d_{k,j,i}$ is the distance between the i -th IoT device and the j -th satellite in the k -th tier,

$$d_{k,j,i} = \sqrt{R_\oplus^2 + R_k^2 - 2R_\oplus R_k \cos \theta_{k,j,i}}, \quad (1)$$

where $\theta_{k,j,i}$ is the central angle between the i -th IoT device and the j -th satellite. An example of the central angle is shown in Fig. 2.

We adopt the Shadowed-Rician distribution to model small-scale fading, as it provides a realistic and precise approximation of satellite-terrestrial channels, accurately capturing small-

TABLE I: Notations and Abbreviations

Symbol/Abbr.	Description
LEO	Low Earth Orbit
PLS	Physical Layer Security
SG	Stochastic Geometry
AN	Artificial Noise
BPP	Binomial Point Process
PPP	Poisson Point Process
LS	Legitimate Satellite
ES	Eavesdropper Satellite
$\Phi_{S_k} \equiv \{\mathbf{x}_{kj}\}$	BPP for satellites in k -th tier
$\Phi_u \equiv \{\mathbf{u}_i\}$	PPP for IoT devices locations
$\mathcal{A}_{m,\text{vis}}$	Visibility area for the m -th tier
\mathcal{I}_m	Interference power for the serving LS at tier m
\mathcal{I}_{kj}	Interference power for j -th ES at tier k
$\mathcal{L}_{\mathcal{I}}(\cdot)$	Laplace transform of the interference \mathcal{I}
$\mathcal{P}_{m,\text{av}}$	Availability probability for m -th tier
$\mathcal{P}_{m,\text{cov}}$	Coverage probability for m -th tier
$\mathcal{P}_{m,\text{suc}}$	Successful communication probability for m -th tier
\mathcal{P}_{out}	Secrecy outage probability
\mathcal{P}_{sec}	Secure communication probability

scale variations and reflecting real-world conditions [23], [44], [45]. Thus, the small-scale fading component, represented by $|h_{k,j,i}|^2$, follows the Shadowed-Rician distribution, which describes the fading between the i -th IoT device and the j -th satellite in the k -th tier.

Combining these components, the received signal power P_{rec} , at the satellite during uplink transmission is modeled as

$$P_{\text{rec}}(d_{k,j,i}) = P_t \left(\frac{c}{4\pi f_c d_{k,j,i}} \right)^2 G |h_{k,j,i}|^2, \quad (2)$$

where P_t denotes the transmit power of the IoT device, G is the product of the gains of the transmitting and receiving antennas.

Next, we determine the range for the central angle θ . Firstly, we consider that IoT devices located within the satellite receiving beam's main lobe can establish a stable link with the satellite. The satellite beam is pointed towards the center of the Earth, and the main lobe angle of the receiving beam is denoted as $2\theta_{\text{beam}}$. As illustrated in Fig. 2, θ_{beam} is the half beamwidth angle of the satellite. In addition, assuming that only satellites with line-of-sight links established with IoT devices can communicate, the upper bound of the central angle can be represented as,

$$\theta_{k,\text{max}} = \begin{cases} \sin^{-1} \left(\frac{R_k}{R_{\oplus}} \sin \theta_{\text{beam}} \right) - \theta_{\text{beam}}, & \theta_{\text{beam}} < \sin^{-1} \left(\frac{R_{\oplus}}{R_k} \right), \\ \cos^{-1} \left(\frac{R_{\oplus}}{R_k} \right), & \theta_{\text{beam}} \geq \sin^{-1} \left(\frac{R_{\oplus}}{R_k} \right), \end{cases} \quad (3)$$

and the range for θ is $0 < \theta < \theta_{k,\text{max}}$.

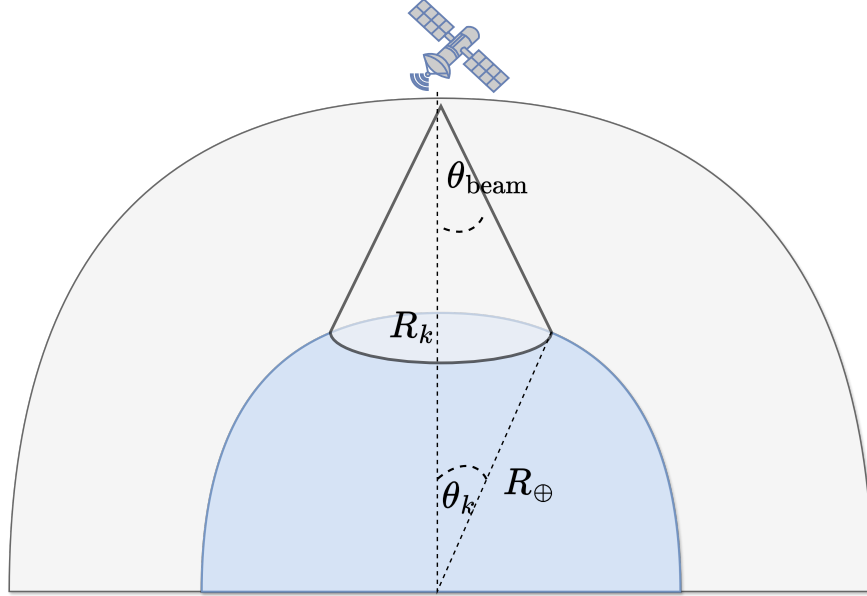


Fig. 2: Illustration of satellite beamwidth θ_{beam} and its impact on Earth's surface coverage.

As mentioned earlier, the Shadowed-Rician distribution is used to model small-scale fading. However, due to the complexity of deriving closed-form solutions from the Shadowed-Rician channel model, we adopt the Gamma fading model as a practical approximation for the Shadowed-Rician fading [35]. Thus, the Cumulative Distribution Function (CDF) of small-scale fading $|h|^2$ is tightly bounded by as follows

$$F_{|h|^2}(x) \leq \left[1 - \exp\left(-\frac{(m_1!)^{-\frac{1}{m_1}}}{m_2} x\right) \right]^{m_1} \quad \text{if } m_1 \leq 1, \quad (4)$$

where m_1 and m_2 denote shape and scale parameters, respectively.

C. Artificial Noise

In this article, we introduce AN into the transmitted signal to enhance its secrecy. The transmit power of IoT device, P_t , is divided into two parts: a fraction γP_t is allocated for transmitting confidential information, $(1 - \gamma) P_t$ is dedicated to transmitting AN. γ is known as the information-bearing ratio, which falls within the interval $[0, 1]$. In scenarios where $\gamma = 1$, AN is not applied, and all of the IoT device's transmit power is dedicated to signal transmission.

Then, we can present the communication links into the legitimate link (typical IoT device to LS), eavesdropping link (typical IoT device to ES), and interfering link (interfering IoT device to the satellite of interest). Due to LSs knowing in advance that typical IoT devices employ AN

strategies, the AN can be filtered out by LSs. When the IoT device is served by the m -th tier, the signal-to-interference and noise ratio (SINR) attained at the serving satellite is expressed as

$$\text{SINR}_{\text{LS}} = \frac{\gamma P_{\text{rec}}(d_{m0,0})}{\mathcal{I}_m + \sigma_{\text{S}}^2}, \quad (5)$$

where $P_{\text{rec}}(d_{m0,i})$ represents the received power at the serving satellite from both typical ($i = 0$) and interfering ($i \neq 0$) devices, with the distance function $d_{m0,i}$ defined in (1). For notation simplicity, and because all IoT devices (typical or interfering) communicate only with the serving satellite in the legitimate tier m , the subscript 0 used for the serving satellite is omitted from $d_{m0,i}$ in favor of $d_{m,i}$, $\forall i$. The noise power at the satellite is denoted by $\sigma_{\text{S}}^2 = N_0 \times B$, where N_0 is the noise spectral density and B is the bandwidth. Furthermore,

$$\mathcal{I}_m = \sum_{i \in \Phi_u \setminus \{i=0\}} P_{\text{rec}}(d_{m,i}) \quad (6)$$

denotes the cumulative interference from other IoT devices ($i \neq 0$) at the serving satellite.

ESs, in contrast, are incapable of filtering out the AN. For the j -th ES located in the k -th tier ($\forall k \neq m$), the SINR of the eavesdropping link is given by

$$\text{SINR}_{kj} = \frac{\gamma P_{\text{rec}}(d_{kj,0})}{(1 - \gamma)P_{\text{rec}}(d_{kj,0}) + \mathcal{I}_{kj} + \sigma_{\text{S}}^2}, \quad (7)$$

where $P_{\text{rec}}(d_{kj,i})$ indicates the received power at the eavesdropper from both typical ($i = 0$) and interfering ($i \neq 0$) IoT devices.

$$\mathcal{I}_{kj} = \sum_{i \in \Phi_u \setminus \{i=0\}} P_{\text{rec}}(d_{kj,i}) \quad (8)$$

represents the total interference from other IoT devices ($i \neq 0$) at the ES.

In conclusion, the addition of AN considerably impairs the eavesdropper's ability to intercept the communication while leaving the reception for the intended receiver unaffected. By carefully managing the power of the AN, it is feasible to markedly improve the confidentiality of uplink transmissions from IoT devices to LEO satellites, thereby enhancing security at the physical layer.

III. PERFORMANCE ANALYSIS

In secure satellite communications, evaluating the effectiveness of PLS techniques requires a comprehensive understanding of how well the system can maintain connectivity, protect against eavesdropping, and ensure reliable and secure data transmission. The performance metrics, availability probability, coverage probability, and secure connection probability are integral to

assessing these aspects. The multi-tier architecture is central to our analysis, enabling us to model various orbital configurations and assess their impacts on key performance metrics. This approach allows evaluation under different conditions, including potential eavesdropping scenarios, highlighting its significance in optimizing secure communication in LEO satellite-enabled IoT networks. In this section, we evaluate the security of the considered system network using the above performance metrics or their combination and provide analytical expressions for these performance metrics.

To facilitate analysis, we begin by characterizing the distribution of the central angle from the typical IoT device to the serving satellite, which is known as the contact angle [46]. Given that N_m satellites are modeled uniformly as BPP, it follows that any randomly chosen points share an identical distribution of the contact angle. Therefore, the CDF and Probability Density Function (PDF) of the contact distance can be articulated in the following lemma.

Lemma 1 (Contact Angle Distribution). *Given the typical IoT device and the closest satellite within the m -th tier, the CDF of the contact angle $\theta_{m,0}$ is given by*

$$F_{\theta_{m,0}}(\theta) = 1 - \left(\frac{1 + \cos \theta}{2} \right)^{N_m}, \quad 0 < \theta < \theta_{m,\max}, \quad (9)$$

and the corresponding PDF is

$$f_{\theta_{m,0}}(\theta) = \frac{N_m \sin \theta}{2} \left(\frac{1 + \cos \theta}{2} \right)^{N_m-1}, \quad 0 < \theta < \theta_{m,\max}, \quad (10)$$

where $\theta_{m,\max}$ is defined in (3).

Proof: See appendix A. ■

Next, we derive the availability probability, which is directly related to the contact angle distribution. The availability probability stands as a fundamental metric, establishing the foundational viability of any communication attempt. Without satellite availability, neither data transmission nor secure communication can occur, as defined and mathematically presented as follows:

Definition 1. *Availability probability is the probability that, within the visible area of a typical IoT device, at least one satellite from the m -th tier is available for communication. It is mathematically presented as follows:*

$$\mathcal{P}_{m,\text{av}} \triangleq \mathbb{P}[\mathcal{N}(\mathcal{A}_{m,\text{vis}}) > 0], \quad (11)$$

where $\mathcal{A}_{m,\text{vis}}$ is the surface area from which satellites at tier m are visible to the typical IoT device, defined by the set $\mathcal{A}_{m,\text{vis}} = \{R_m, 0 \leq \theta \leq \theta_{m,\max}, 0 \leq \varphi \leq 2\pi\}$. $\mathcal{N}(\mathcal{A}_{m,\text{vis}})$ counts the number

of satellites in the surface area $\mathcal{A}_{m,\text{vis}}$.

Next, we derive the availability probability in the following lemma as defined in Definition 1, which is directly related to the contact angle distribution.

Lemma 2 (Availability Probability). *The probability of availability $\mathcal{P}_{m,\text{av}}$ of a satellite in the m -th tier is given as*

$$\mathcal{P}_{m,\text{av}} = 1 - \left(\frac{1 + \cos \theta_{m,\text{max}}}{2} \right)^{N_m}, \quad (12)$$

where $\theta_{m,\text{max}}$ is defined in (3) and N_m is the total number of satellites within tier m .

Proof: Essentially, the CDF of contact angle distribution, which is defined as $\mathbb{P}[\theta_{m,0} < \theta]$ is equivalent to the availability probability $\mathbb{P}[\mathcal{N}(\mathcal{A}_{m,\text{vis}}) = 0]$, when $\theta_{m,0} = \theta_{m,\text{max}}$, where $\mathcal{A}_{m,\text{vis}}$ describes the maximum visibility area. Following the void probability, the lemma is proved. ■

Once the availability of satellites is determined, the analysis progresses to the coverage probability. Coverage probability assesses the likelihood that a communication link, specifically between a typical IoT device and its serving satellite, can be established with sufficient signal quality. This quality is necessary to decode transmitted signals with minimal errors accurately. It is conditional upon the SINR exceeding a predetermined threshold, β_{LS} and is defined as follows:

Definition 2. *The coverage probability is the probability that the SINR for the legitimate link is greater than β_{LS} , thereby ensuring reliable signal decoding. Formally, it is expressed as:*

$$\mathcal{P}_{m,\text{cov}} \triangleq \mathbb{P}[\text{SINR}_{\text{LS}} > \beta_{\text{LS}}], \quad (13)$$

where the SINR_{LS} is defined in (5).

Prior to the analysis of coverage probability, we need to understand the impact of interference on the communication link. Given the spatial distribution of IoT devices follows PPP, we employ the Laplace Transform (LT) to obtain more manageable and closed-form expressions for interference analysis.

Lemma 3 (Laplace Transform of Interference). *For a given satellite located in tier m , the LT of the interference $\mathcal{L}_{I_m}(s)$ experienced by this satellite is:*

$$\mathcal{L}_{I_m}(s) = \exp \left(-\lambda_u \int_0^{2\pi} \int_0^{\theta_{m,\text{max}}} \left[1 - \left(1 + m_2 s P_t G \left(\frac{c}{4\pi f d} \right)^2 \right)^{-m_1} \right] R_{\oplus}^2 \sin \theta d\theta d\varphi \right),$$

where $\theta_{m,\text{max}}$ is defined in (3).

Proof: See appendix B. ■

Building upon the interference analysis, the derivation of the coverage probability proceeds as follows.

Lemma 4 (Coverage Probability). *The coverage probability for the uplink communication between a typical IoT device and its nearest LS in the m -th tier with SINR threshold β_{LS} is derived as follows:*

$$\mathcal{P}_{m,\text{cov}} = \sum_{q=1}^{m_1} \binom{m_1}{q} (-1)^{q+1} \int_0^{\theta_{m,\text{max}}} \exp(-qs_{\text{LS}}\sigma_s^2) \mathcal{L}_{\mathcal{I}_m}(qs_{\text{LS}}) f_{\theta_{m,0}}(\theta) d\theta,$$

where $s_{\text{LS}} = \frac{(m_1!)^{-\frac{1}{m_1}} \beta_{\text{LS}}}{m_2 \gamma P_t G} \left(\frac{4\pi f d_{m,0}}{c} \right)^2$, and $\theta_{m,\text{max}}$ is as defined in (3). The functions $f_{\theta_{m,0}}(\cdot)$, $\mathcal{P}_{m,\text{av}}$, and $\mathcal{L}_{\mathcal{I}_m}(\cdot)$ are provided in Lemma 1, Lemma 2 and Lemma 3, respectively.

Proof: See appendix C. ■

We are ready to introduce the concept of successful communication probability, one of the main metrics, which involves the insights gained from the availability and coverage probabilities. The successful communication probability denoted as $\mathcal{P}_{m,\text{suc}}$, is defined as the probability that an uplink connection made by the typical IoT device to its nearest satellite in the m -th tier successfully meets both availability and coverage criteria. Mathematically, this probability is expressed as the product of the availability probability and the coverage probability:

$$\mathcal{P}_{m,\text{suc}} = \mathcal{P}_{m,\text{av}} \times \mathcal{P}_{m,\text{cov}}, \quad (14)$$

where $\mathcal{P}_{m,\text{av}}$ and $\mathcal{P}_{m,\text{cov}}$ are derived in Lemma 2 and Lemma 4, respectively.

Moving beyond the feasibility of communication, the definition of secrecy outage probability addresses the security aspect, which investigates the scenario where the SINR experienced by any potential ES falls below a certain predefined threshold, β_{ES} . Hence, within a multi-tiered satellite constellation framework, we define and derive the secrecy outage probability as follows.

Definition 3. *Secrecy outage probability is the probability that the highest SINR experienced by any ES across a multi-tiered satellite constellation falls below a predefined threshold β_{ES} . Mathematically, \mathcal{P}_{out} is defined as:*

$$\mathcal{P}_{\text{out}} \triangleq \mathbb{P} \left[\max_{k \neq m} \max_{j \in \Phi_{S_k}} \{ \text{SINR}_{kj} \} < \beta_{\text{ES}} \right], \quad (15)$$

where SINR_{kj} represents the SINR experienced by j -th ES within the k -th tier, excluding the

legitimate m -th tier , where the expression is given in (7).

Upon the definition of the secrecy outage probability, we can derive the expression of the \mathcal{P}_{out} in the following lemma.

Theorem 1 (Secrecy Outage Probability). *For a given value of β_{ES} , the probability of secrecy outage, as defined in Definition 3, is derived as:*

$$\mathcal{P}_{\text{out}} = \prod_{\substack{k=1 \\ k \neq m}}^K \left[\sum_{q=0}^{m_1} \binom{m_1}{q} (-1)^q \int_0^{\theta_{k,\max}} \exp(-qs_{\text{ES}}\sigma_S^2) \mathcal{L}_{\mathcal{I}_{kj}}(qs_{\text{ES}}) \times f_{\theta_{k,0}}(\theta) d\theta + \frac{1 + \cos \theta_{k,\max}}{2} \right]^{N_k},$$

with $s_{\text{ES}} = \frac{(m_1!)^{-\frac{1}{m_1}}}{m_2} \frac{\beta_{\text{ES}}}{[\gamma - \beta_{\text{ES}}(1-\gamma)]P_{tG}} \left(\frac{4\pi f d_{k,j,0}}{c} \right)^2$ and $f_{\theta_{k,0}}(\theta) = \frac{\sin \theta}{2}$. The LT of interference, $\mathcal{L}_{\mathcal{I}_{kj}}(\cdot)$, is derived in Lemma 3.

Proof: See appendix D. ■

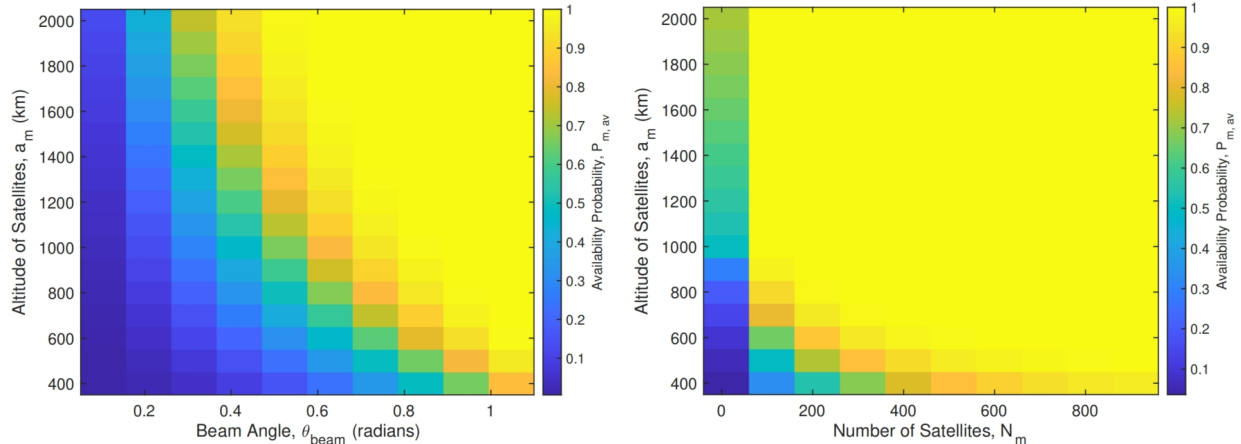
Finally, our contribution goes further by not only considering the successful connection but also ensuring the data transmitted is secure from eavesdropping. The secure communication probability, denoted as \mathcal{P}_{sec} , is calculated as the product of two key factors: the probability of the typical IoT device achieving successful communication within the legitimate m -th tier and the secrecy outage probability considering the influence of all ES. Mathematically, the secure communication probability is formulated as:

$$\mathcal{P}_{\text{sec}} = \mathcal{P}_{m,\text{suc}} \times \mathcal{P}_{\text{out}}, \quad (16)$$

where \mathcal{P}_{out} , the secrecy outage probability is elaborated on in Theorem 1, and $\mathcal{P}_{m,\text{suc}}$, the probability of achieving successful communication, is described in (14).

IV. NUMERICAL RESULTS

In this section, we present numerical results for the derived performance metrics. We employed Monte Carlo simulations with 10,000 iterations. In each iteration, the positions of the satellites and IoT devices were varied to simulate the dynamic changes in the topology. This approach ensures that the performance metrics derived from our analytical expressions correspond to the average performance of the network under dynamic conditions rather than a static snapshot. We use lines to present analytical results and markers to present Monte Carlo simulation results. The matching between them in the figures provided in this section aims to affirm the accuracy of our analysis further. The parameters employed in these simulations are detailed in Table II.



(a) $\mathcal{P}_{m,av}$ against beamwidth angle and the altitude of satellites (b) $\mathcal{P}_{m,av}$ against number of satellites and the altitude of satellites

Fig. 3: Heat map representing the $\mathcal{P}_{m,av}$ for different parameters of satellite network.

TABLE II: Simulation Parameters

Notation	Parameter	Default Value
f_c	Center frequency	2 GHz
R_{\oplus}	Earth radius	6371 km
N_k	Number of satellites in tier k , $\forall k$	500
a_k	Altitude of satellites for all tier, $k = 1, 2, 3$	[500, 1000, 1500] km
θ_{beam}	Half beamwidth angle of satellite	$\pi/3$
P_t	Uplink transmit power of IoT devices	23 dBm
λ_u	Density of users (IoT devices)	10^{-6} devices/km ²
N_0	Noise spectral density	-174 dBm/Hz
B	Bandwidth	180 KHz
$\Gamma(m_1, m_2)$	Gamma shape and scale parameters	$[m_1, m_2] = [1, 0.1269]$
γ	AN power allocation coefficient	0.1
G	Antenna bea, gain	41.9 dBi
β_{ES}	SINR threshold at ES	-10 dB
β_{LS}	SINR threshold at LS	-30 dB

A. System Design on Network Availability

This subsection provides how the design of satellite networks influences a network's ability to establish communication links between IoT devices and satellites. As shown in (12), the availability probability $\mathcal{P}_{m,av}$ is influenced by the beamwidth, number, and altitude of satellites. In Fig. 3, we highlight the optimal parameters design with regard to $\mathcal{P}_{m,av}$.

In Fig. 3(a), as the beamwidth angle increases, the area covered by each satellite's communication beam expands, increasing the availability probability $\mathcal{P}_{m,av}$. Furthermore, with the same beam angle, satellites at higher altitudes cover a larger area of the Earth's surface, thus increasing $\mathcal{P}_{m,av}$. With a fixed constellation size (e.g., $N_m = 500$), we observe that we can reach $\mathcal{P}_{m,av} \approx 1$

for satellite altitudes higher than 500 km when the beamwidth angle is set to $\theta_{\text{beam}} = \frac{\pi}{3}$.

Fig. 3(b) demonstrates how $\mathcal{P}_{m,\text{av}}$ is influenced by constellation configurations. Increasing the number and altitude of satellites can enhance $\mathcal{P}_{m,\text{av}}$. The analysis identifies a constellation size of $N_m = 500$ satellites as particularly effective in securing near-universal availability across all network tiers with $\mathcal{P}_{m,\text{av}} \approx 1$. Further increasing the number of satellites offers limited benefits to availability.

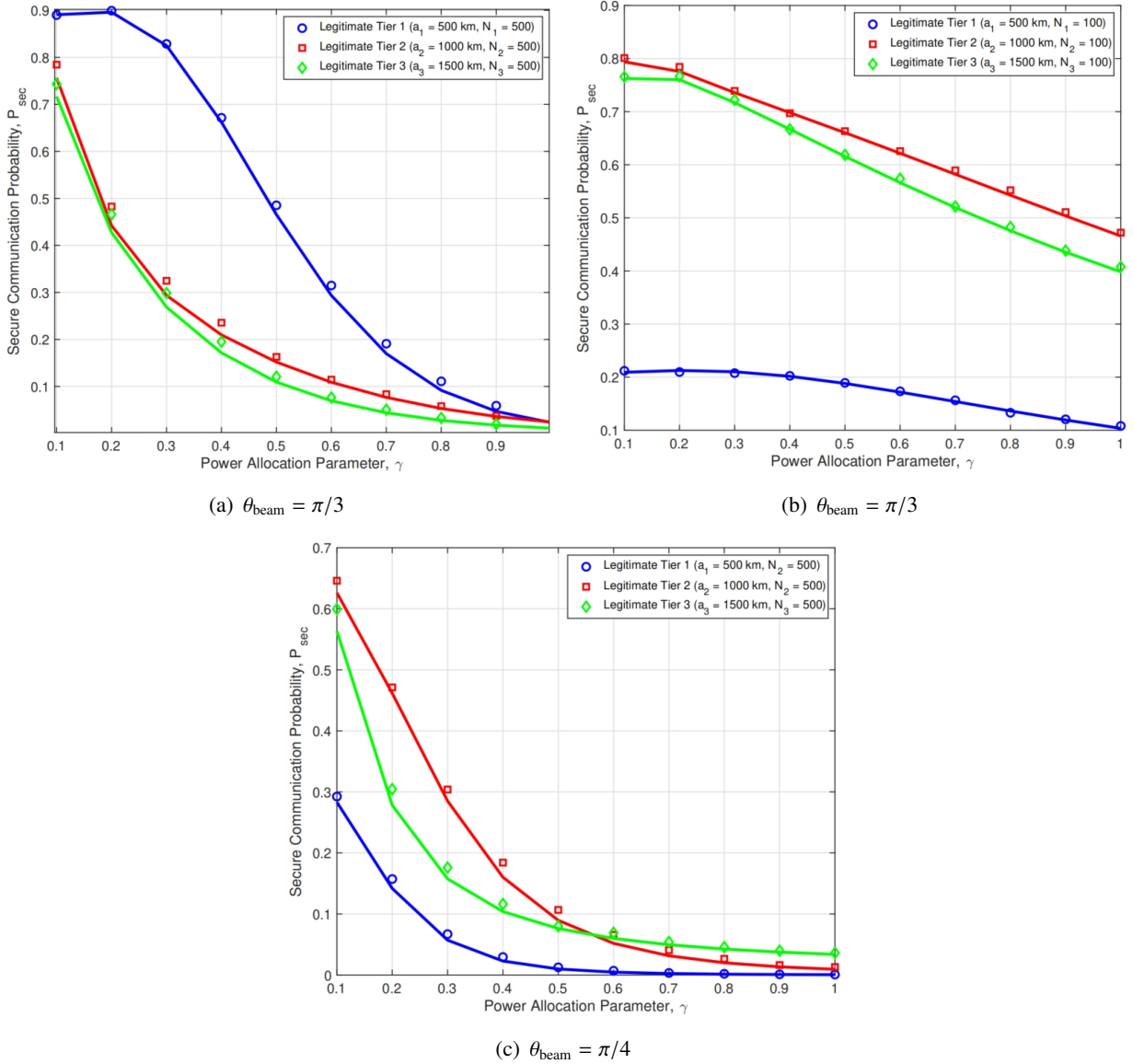


Fig. 4: The effects of power allocation across three configurations on \mathcal{P}_{sec} .

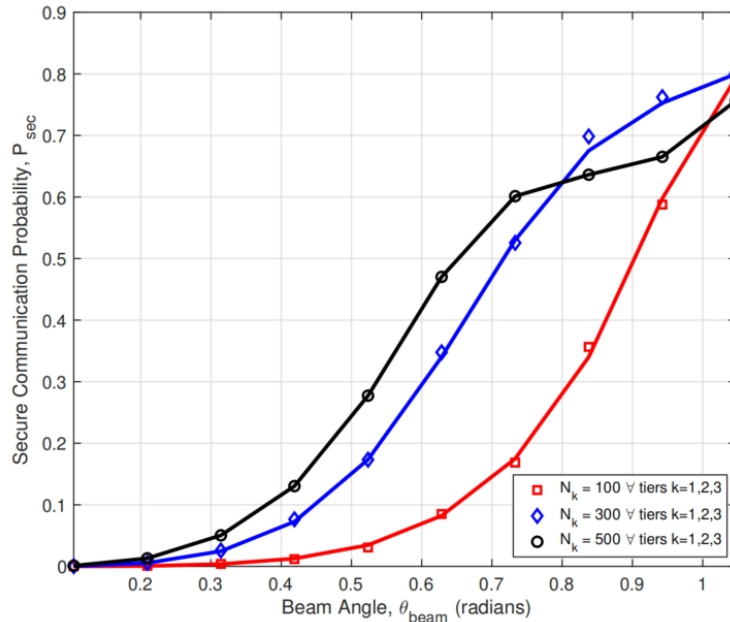


Fig. 5: Impact of satellite numbers on \mathcal{P}_{sec} against beam angle.

B. Enhancing PLS: Techniques and Trade-offs

This subsection discusses how different strategies can influence the secure communication probability \mathcal{P}_{sec} . Unless otherwise stated, we adopt a 3-tier constellation, with altitudes set at $a_S = [500, 1000, 1500]$ km. The number of satellites for all tiers is fixed as $N_k = 500, \forall k = 1, 2, 3$.

Fig. 4 shows how different choices of the legitimate tier and the power allocation parameter γ influence \mathcal{P}_{sec} . We observe a consistent trend across all subfigures: \mathcal{P}_{sec} decreases as γ increases. This is because less power is allocated to AN for a higher γ , making it easier for eavesdroppers to decode the signal. More precisely, the transition from Fig. 4(a) to Fig. 4(b) and Fig. 4(c) illustrates changes in satellite number and beam angle. When the satellite count is increased, the chance of having a satellite available for communication ($\mathcal{P}_{m,\text{av}}$) is high, leading to Tier-1 having the highest \mathcal{P}_{sec} as depicted in Fig. 4(a). However, more satellites can also create more interference, particularly at higher altitudes, thus lowering \mathcal{P}_{sec} in Tiers 2 and 3. Conversely, in Fig. 4(b), reducing the number of satellites significantly impacts Tier-1, making it less secure due to a lower $\mathcal{P}_{m,\text{av}}$; thus, Tier-2 becomes the preferred choice for the legitimate tier due to its balanced performance. Fig. 4(c) shows the effects of reducing beam angle from $\theta_{\text{beam}} = \frac{\pi}{3}$ to $\theta_{\text{beam}} = \frac{\pi}{4}$ while maintaining $N_k = 500, \forall k$. In this configuration, Tiers 2 and 3 outperform Tier 1 across the entire range of the γ . The narrower beam angle implies a need for more satellites to maintain high $\mathcal{P}_{m,\text{av}}$. Overall, we can draw the same conclusion because whether reducing N_k

$\forall k$, or θ_{beam} decreases the $\mathcal{P}_{m,\text{av}}$.

The adjustments illustrate a trade-off between availability and signal quality, indicating that Tier-2, with an altitude of $a_m = 1000$ km, is the optimal choice for the legitimate tier due to its consistently stable maximum \mathcal{P}_{sec} as depicted in Fig. 4. Therefore, unless otherwise stated, subsequent analyses of system performance in Figs. 5, 6, and 7 focus on Tier-2 as the legitimate tier.

Fig. 5 highlights the nuanced impact of varying satellite numbers and beam angles on \mathcal{P}_{sec} . A key trade-off emerges in the number of satellites: more satellites can improve coverage and security up to a point, but beyond that, they might introduce excessive interference or potential eavesdroppers. In this case, we should emphasize the need for an optimized satellite constellation design.

Moving to Fig. 6, as γ increases, the behaviour of \mathcal{P}_{sec} is totally differently for the three densities of IoT devices. For the sparsest IoT network ($\lambda_u = 10^{-6}$), \mathcal{P}_{sec} exhibits a peak at lower γ values. When interference is negligible, allocating more power to AN can effectively protect the PLS. In contrast, in the high-density scenario ($\lambda_u = 10^{-4}$), an inverse trend is observed where \mathcal{P}_{sec} is the lowest at $\gamma = 0.1$ but increases steadily. This trend reflects that ensuring the information can effectively reach LSs in an interference-limited scenario is more important than preventing eavesdropping. When $\lambda_u = 10^{-5}$, the trend of \mathcal{P}_{sec} initially rising and then declining suggests that balancing between ensuring successful, legitimate communication and preventing eavesdropping is crucial. In summary, Fig. 6 highlights a critical density-dependent optimization strategy for allocating power between messaging and AN to maximize the \mathcal{P}_{sec} .

C. Security Performance Optimization

In this subsection, we explore adjustments to the network configuration and security outcomes to maximize or achieve optimal security.

Fig. 7 visually represents the optimization of \mathcal{P}_{sec} in sparse ($\lambda_u = 10^{-6}$) versus denser ($\lambda_u = 10^{-5}$) IoT devices deployment. There is a clear distinction in how θ_{beam} and γ influence \mathcal{P}_{sec} at different device densities. As shown in Fig. 7(a), for lower density ($\lambda_u = 10^{-6}$), \mathcal{P}_{sec} is more sensitive to the configuration of θ_{beam} and γ , favoring wider beam angles and a large share of power dedicated to AN. This indicates that securing communications relies more on AN in environments with fewer devices, with a wider signal spread proving beneficial due to the lower interference risk. Conversely, Fig. 7(b) corresponds to a denser network ($\lambda_u = 10^{-5}$), shows a

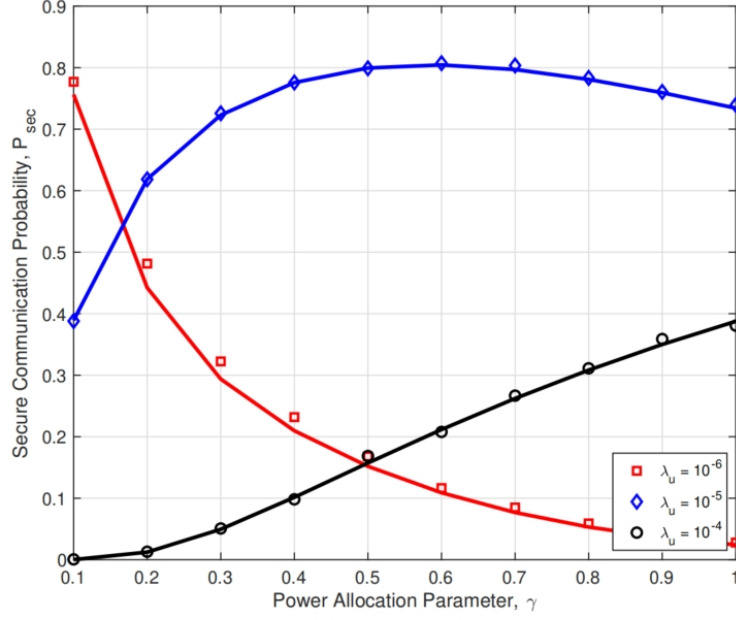


Fig. 6: \mathcal{P}_{sec} as a function of power allocation parameter across different densities of IoT devices.

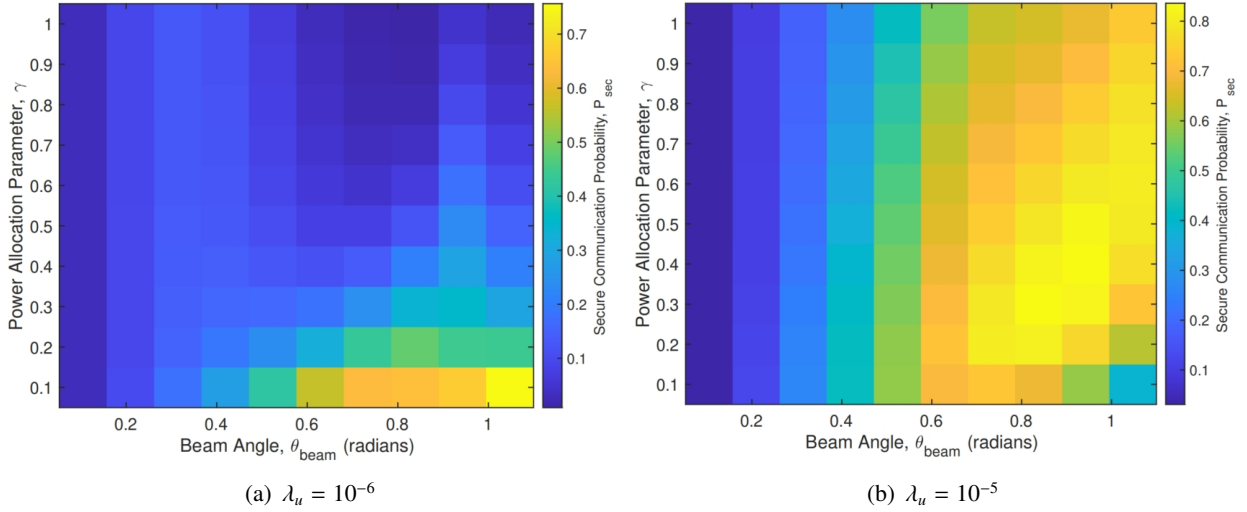


Fig. 7: Optimal beam angle and AN power allocation for maximizing \mathcal{P}_{sec} in different IoT devices.

different trend, where \mathcal{P}_{sec} demonstrates reduced sensitivity to variations in γ , especially at lower beam angles. The optimal \mathcal{P}_{sec} levels, as indicated by a yellow gradient, are observed across a broader range of beam angles compared to Fig. 7(a). This pattern suggests that high-security levels are attainable with a variety of γ settings, with the yellow regions extending throughout the full range of γ values from low to high.

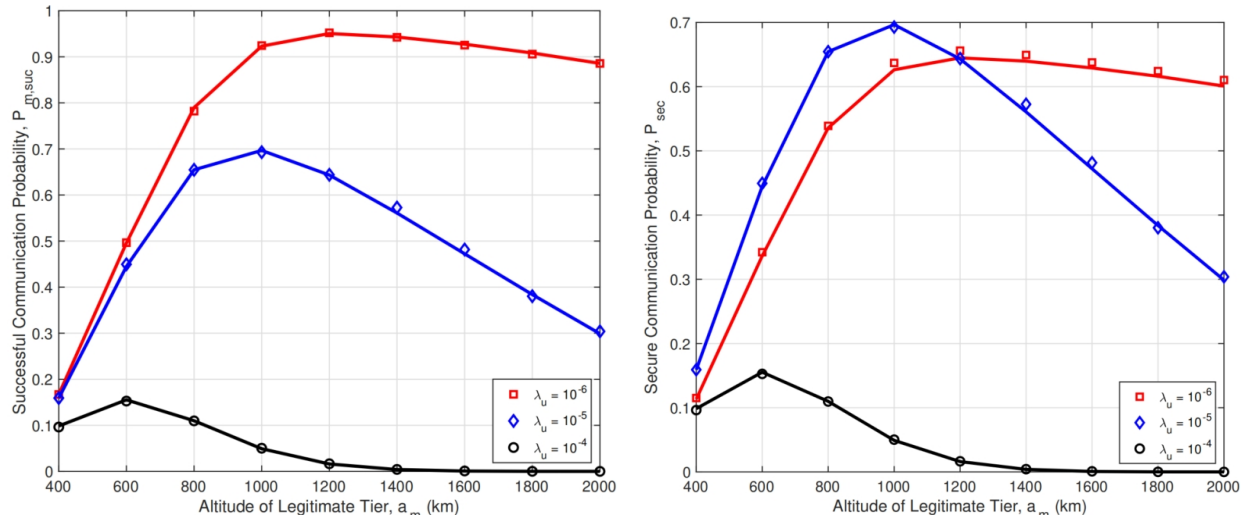


Fig. 8: Impact of the LS altitude on $\mathcal{P}_{m,suc}$ and \mathcal{P}_{sec} across different IoT device densities.

Overall, lower-density environments show the highest secrecy with significant AN, while higher-density environments maintain high secrecy across varying levels of AN power.

In Fig. 8, we explore the effects of varying altitudes in the legitimate tier while keeping the altitudes of the potential eavesdropping tiers fixed at 500 and 1500 km. The optimal altitude exists for both $\mathcal{P}_{m,suc}$ and \mathcal{P}_{sec} across varying densities of IoT devices. Specifically, the optimal legitimate altitude decreases as the density increases. At very high densities, the optimal altitude is found to be 600 km. As the density decreases slightly, this optimal altitude increases to 1000 km, and with a further reduction in density, it reaches 1200 km. This is the result of a trade-off between availability and received signal strength. In most cases, as the density of IoT devices increases, $\mathcal{P}_{m,suc}$ and \mathcal{P}_{sec} tends to decrease. When $\lambda_u = 10^{-5}$, \mathcal{P}_{sec} presents more nuanced results. We interpret this interesting phenomenon as interference protecting signal security. This protective mechanism is similar to AN technology, where the received SINR of LSs is sacrificed to introduce more interference to eavesdroppers. However, this trade-off has its limits, as demonstrated by the highest density ($\lambda_u = 10^{-4}$), which does not yield any beneficial impact on \mathcal{P}_{sec} . This suggests a threshold beyond which additional interference no longer benefits securing communications.

V. CONCLUSION

In conclusion, this paper represents a significant advancement in securing IoT communications via LEO satellites by implementing PLS strategies enhanced by SG tools and AN techniques. The primary contribution of this study lies in its innovative approach to modeling the spatial

distribution of legitimate and ESs as well as IoT devices. This enables a more accurate analysis of security threats and the effectiveness of PLS measures within a LEO satellite-enabled IoT network. By integrating AN into the PLS framework and utilizing SG for network analysis, this research not only addresses the substantial security challenges presented by the extensive coverage and accessibility of LEO satellites but also provides a scalable solution capable of adapting to the dynamic nature of satellite positions and fluctuating channel conditions. However, the trade-off analysis suggests that while the proposed model significantly enhances security, careful management of AN is required to prevent compromising communication integrity. Furthermore, the model operates under the assumption of known eavesdropper altitudes, which may not always be applicable in practical scenarios. Nonetheless, these findings offer valuable insights into ongoing efforts to secure satellite-based IoT networks, proposing avenues for future research to enhance the robustness and applicability of PLS solutions in such complex and evolving communication environments.

APPENDIX A

PROOF OF LEMMA 1

We consider the spatial distribution of satellites within a homogeneous BPP across the surface of a sphere; we focus on the m -th tier (i.e., the sphere S_m) to ascertain the distribution characteristics of the nearest satellite. Within this framework, the probability $\mathbb{P}[\theta_{m,0} \leq \theta]$ that a randomly chosen satellite falls within a spherical cap defined by a central angle θ is proportional to the area of this cap relative to the sphere's total surface area. Mathematically, this probability is given by:

$$\mathbb{P}[\theta_{m,0} \leq \theta] = \frac{\mathcal{S}(\mathcal{A}_{m,\text{vis}})}{\mathcal{S}(\mathcal{A}_{S_m})} = \frac{2\pi R_m^2(1 - \cos \theta)}{4\pi R_m^2}.$$

Simplifying, we find:

$$\mathbb{P}[\theta_{m,0} \leq \theta] = \frac{1 - \cos \theta}{2}.$$

The CDF for the contact angle $F_{\theta_{m,0}}(\theta)$, considers the case where the serving satellite is the nearest among all N_m i.i.d. satellites and derived easily as follows

$$F_{\theta_{m,0}}(\theta) = 1 - \prod_1^{N_m} \mathbb{P}[\theta_{m,0} > \theta] = 1 - \left[1 - \frac{1 - \cos \theta}{2}\right]^{N_m}.$$

This equation captures the probability that at least one satellite is within the spherical cap, effectively accounting for the presence of N_m satellites in the calculation. The PDF can be obtained by differentiating the CDF with respect to θ .

APPENDIX B
PROOF OF LEMMA 3

Recall that the interference is expressed as

$$\mathcal{I}_m = \sum_{i \in \Phi_u \setminus \{i=0\}} P_t \left(\frac{c}{4\pi f d_{m,i}} \right)^2 G |h_{m,i}|^2, \quad (17)$$

where the $d_{m,i}$ is the distance between the serving LS with the interfering i -th IoT device. We proceed with the derivation of the LT of interference by definition:

$$\begin{aligned} \mathcal{L}_{\mathcal{I}_m}(s) &\triangleq \mathbb{E} \left\{ \exp(-s\mathcal{I}_m) \middle| \theta, \mathcal{I}_m \right\} \\ &= \mathbb{E}_{\Phi_u, \{|h_{m,i}|^2\}} \left\{ \exp \left(-s \sum_{i \in \Phi_u \setminus \{i=0\}} P_t \left(\frac{c}{4\pi f d_{m,i}} \right)^2 G |h_{m,i}|^2 \right) \right\} \\ &\stackrel{(a)}{=} \mathbb{E}_{\Phi_u} \left\{ \prod_{i \in \Phi_u \setminus \{i=0\}} \mathbb{E}_{|h_{m,i}|^2} \left[\exp \left(-s P_t \left(\frac{c}{4\pi f d_{m,i}} \right)^2 G |h_{m,i}|^2 \right) \right] \right\} \\ &\stackrel{(b)}{=} \mathbb{E}_{\Phi_u} \left\{ \prod_{i \in \Phi_u \setminus \{i=0\}} \left(1 + m_2 s P_t G \left(\frac{c}{4\pi f d_{m,i}} \right)^2 \right)^{-m_1} \right\} \\ &\stackrel{(c)}{=} \exp \left(-\lambda_u \int_0^{2\pi} \int_0^{\theta_{m,\max}} \left[1 - \left(1 + m_2 s P_t G \left(\frac{c}{4\pi f d} \right)^2 \right)^{-m_1} \right] \times R_{\oplus}^2 \sin \theta d\phi d\theta \right), \end{aligned}$$

where step (a) stands since the fading distribution $|h_{m,i}|^2$ for each IoT device is i.i.d. and is independent of the interfering point process Φ_u . Step (b) follows the Moment Generating Function (MGF) of the Gamma distribution. Finally, step (c) follows the Probability Generating Functional (PGFL) of the PPP, considering that the interference signal originates from devices within the satellite's coverage area.

APPENDIX C
PROOF OF LEMMA 4

Having already derived the expression for availability probability, we now turn our attention to finalizing the successful communication probability by deriving the coverage probability. As previously noted, under the assumption that tier m represents the legitimate tier, it suffices to derive the expression for $\mathcal{P}_{m,\text{cov}}$, the probability that the predefined threshold is lower than the SINR of the LS. The derivation proceeds as follows:

$$\mathcal{P}_{m,\text{cov}} \triangleq \mathbb{P} [\text{SINR}_{\text{LS}} > \beta_{\text{LS}}]$$

$$\begin{aligned}
&\stackrel{(a)}{=} \mathbb{P} \left[\frac{\gamma P_t \left(\frac{c}{4\pi f d_{m,0}} \right)^2 G |h_{m,0}|^2}{\mathcal{I}_m + \sigma_S^2} > \beta_{\text{LS}} \right] \\
&= \mathbb{E}_{\theta, \mathcal{I}_m} \left\{ 1 - F_{|h_{m,0}|^2} \left(\frac{\beta_{\text{LS}} (\mathcal{I}_m + \sigma_S^2)}{\gamma P_t G} \left(\frac{4\pi f d_{m,0}}{c} \right)^2 \right) \right\} \\
&\stackrel{(b)}{\approx} \mathbb{E}_{\theta, \mathcal{I}_m} \left\{ 1 - \left[1 - \exp \left(-\frac{(m_1!)^{-\frac{1}{m_1}} \beta_{\text{LS}}}{m_2 \gamma P_t G} \left(\frac{4\pi f d_{m,0}}{c} \right)^2 \right. \right. \right. \\
&\qquad \qquad \qquad \left. \left. \left. \times (\mathcal{I}_m + \sigma_S^2) \right) \right] \right\}^{m_1} \\
&\stackrel{(c)}{=} \mathbb{E}_{\theta, \mathcal{I}_m} \left\{ 1 - \sum_{q=0}^{m_1} \binom{m_1}{q} (-1)^q \exp(-s_{\text{LS}} q (\mathcal{I}_m + \sigma_S^2)) \right\} \\
&\stackrel{(d)}{=} \sum_{q=1}^{m_1} \binom{m_1}{q} (-1)^{q+1} \int_0^{\theta_{m,\max}} \exp(-q s_{\text{LS}} \sigma_S^2) \mathcal{L}_{\mathcal{I}_m}(q s_{\text{LS}}) f_{\theta_{m,0}}(\theta) d\theta,
\end{aligned}$$

where step (a) is derived by direct expansion of the definition in (5), step (b) follows the upper bound for the CDF of the Gamma function detailed in (4). This approximation is crucial for simplifying the expression involving the channel gain's distribution, facilitating a more tractable analysis of the coverage probability. Step (c) utilizes Newton's generalized binomial theorem to expand the expression. The scaling factor s in step (c) is defined as:

$$s_{\text{LS}} = \frac{(m_1!)^{-\frac{1}{m_1}} \beta_{\text{LS}}}{m_2 \gamma P_t G} \left(\frac{4\pi f d_{m,0}}{c} \right)^2$$

Finally, step (d) integrates the expectation over the distribution of the contact angle, $\theta_{m,0}$, and the interference model, taking into account the spatial geometry of satellite coverage and the statistical properties of the channel. This concludes the proof.

APPENDIX D

PROOF OF THEOREM 1

To state the final expression of the secure communication probability, it's sufficient to outline the derivation secrecy outage probability. Here, we consider the influence of potential ESs across all tiers, with the exception of the legitimate tier. The objective is to evaluate the maximum SINR experienced by these ESs. Therefore, the secrecy probability of a typical IoT device is defined as the probability that the SINR by all ESs for all tiers is less than threshold β_{ES} . First, we will find the strongest SINR of any tier $k \neq m$ such that

$$\mathcal{P}_{\text{out}} \triangleq \mathbb{P} \left[\max_{k \neq m} \max_{j \in \Phi_{\text{S}_k}} \{ \text{SINR}_{kj} \} < \beta_{\text{ES}} \right]$$

$$\begin{aligned}
& \stackrel{(a)}{=} \prod_{\substack{k=1 \\ k \neq m}}^K \prod_{j=1}^{N_k} \mathbb{P} [\text{SINR}_{kj} < \beta_{\text{ES}}] \\
& \stackrel{(b)}{=} \prod_{\substack{k=1 \\ k \neq m}}^K \left[\int_0^{\theta_{k,\max}} \mathbb{P} [\text{SINR}_k < \beta_{\text{ES}}] f_{\theta_{k,0}}(\theta) d\theta + \int_{\theta_{k,\max}}^{\pi} f_{\theta_{k,0}}(\theta) d\theta \right]^{N_k}
\end{aligned}$$

where step (a) follows from the independence of satellites' positions. Step (b) holds because of the i.i.d. characteristic of the channel fading.

Diving into the probability calculation for a single ES, we manipulate the SINR condition under the constraint $d < d_{\max}$, leading to a form that involves expected values over the contact angle distribution and the interference model. The contact angle distribution defined for each satellite can be derived from Lemma 1 by assuming $N_k = 1$:

$$f_{\theta_{k,0}}(\theta) = \frac{\sin \theta}{2}. \quad (18)$$

Following similar steps to the coverage probability proof, we arrive at the formulation for the integral part of step (b):

$$\begin{aligned}
& \int_0^{\theta_{k,\max}} \mathbb{P} [\text{SINR}_{S_k} < \beta_{\text{ES}}] f_{\theta_{k,0}}(\theta) d\theta \\
& = \sum_{q=0}^{m_1} \binom{m_1}{q} (-1)^q \int_0^{\theta_{k,\max}} \exp(-q s_{\text{ES}} \sigma_S^2) \mathcal{L}_{\mathcal{I}_{kj}}(q s_{\text{ES}}) f_{\theta_{k,0}}(\theta) d\theta
\end{aligned}$$

with s_{ES} defined as:

$$s_{\text{ES}} = \frac{(m_1!)^{-\frac{1}{m_1}}}{m_2} \frac{\beta_{\text{ES}}}{[\gamma - \beta_{\text{ES}}(1 - \gamma)] P_t G} \left(\frac{4\pi f d_{k,j,0}}{c} \right)^2.$$

The second integral part in step (b) can be calculated as:

$$\int_{\theta_{k,\max}}^{\pi} f_{\theta_{k,0}}(\theta) d\theta = \frac{1 + \cos \theta_{k,\max}}{2}.$$

Combining the above results, we articulate the secrecy outage probability (16) as

$$\mathcal{P}_{\text{out}} = \prod_{\substack{k=1 \\ k \neq m}}^K \left[\sum_{q=0}^{m_1} \binom{m_1}{q} (-1)^q \int_0^{\theta_{k,\max}} \exp(-q s_{\text{ES}} \sigma_S^2) \mathcal{L}_{\mathcal{I}_{kj}}(q s_{\text{ES}}) f_{\theta_{k,0}}(\theta) d\theta + \frac{1 + \cos \theta_{k,\max}}{2} \right]^{N_k}.$$

In summary, this proof thoroughly derives the secrecy probability by considering the strongest eavesdropper's SINR across all non-legitimate tiers, effectively encapsulating the multifaceted dynamics of satellite communication systems where secrecy against ESs is paramount.

REFERENCES

- [1] O. Kodheli, E. Lagunas, N. Maturo, S. K. Sharma, B. Shankar, J. F. M. Montoya, J. C. M. Duncan, D. Spano, S. Chatzinotas, S. Kisseleff, J. Querol, L. Lei, T. X. Vu, and G. Goussetis, "Satellite Communications in the New Space Era: A Survey and Future Challenges," *IEEE Communications Surveys and Tutorials*, vol. 23, no. 1, pp. 70–109, 2021.
- [2] Z. Qu, G. Zhang, H. Cao, and J. Xie, "LEO Satellite Constellation for Internet of Things," *IEEE Access*, vol. 5, pp. 18 391–18 401, 2017.
- [3] M. Centenaro, C. E. Costa, F. Granelli, C. Sacchi, and L. Vangelista, "A Survey on Technologies, Standards and Open Challenges in Satellite IoT," *IEEE Communications Surveys and Tutorials*, vol. 23, no. 3, pp. 1693–1720, 2021.
- [4] M. Mitry, "Routers in Space: Kepler Communications' CubeSats Will Create an Internet for Other Satellites," *IEEE Spectrum*, vol. 57, no. 2, pp. 38–43, 2020.
- [5] A. D. Wyner, "The Wire-Tap Channel," *Bell System Technical Journal*, vol. 54, no. 8, pp. 1355–1387, 1975.
- [6] B. Li, Z. Fei, C. Zhou, and Y. Zhang, "Physical-Layer Security in Space Information Networks: A Survey," *IEEE Internet of Things Journal*, vol. 7, no. 1, pp. 33–52, 2020.
- [7] P. Tedeschi, S. Sciancalepore, and R. Di Pietro, "Satellite-Based Communications Security: A Survey of Threats, Solutions, and Research Challenges," *Computer Networks*, vol. 216, p. 109246, 2022.
- [8] S. Han, J. Li, W. Meng, M. Guizani, and S. Sun, "Challenges of Physical Layer Security in a Satellite-Terrestrial Network," *IEEE Network*, vol. 36, no. 3, pp. 98–104, 2022.
- [9] N. Abdelsalam, S. Al-Kuwari, and A. Erbad, "Physical Layer Security in Satellite Communication: State-of-the-Art and Open Problems," 2023, [Online]. Available: <https://arxiv.org/abs/2301.03672>.
- [10] S. Goel and R. Negi, "Guaranteeing Secrecy using Artificial Noise," *IEEE Transactions on Wireless Communications*, vol. 7, no. 6, pp. 2180–2189, 2008.
- [11] M. A. Kishk and H. S. Dhillon, "Stochastic Geometry-Based Comparison of Secrecy Enhancement Techniques in D2D Networks," *IEEE Wireless Communications Letters*, vol. 6, no. 3, pp. 394–397, 2017.
- [12] G. Zheng, P.-D. Arapoglou, and B. Ottersten, "Physical Layer Security in Multibeam Satellite Systems," *IEEE Transactions on Wireless Communications*, vol. 11, no. 2, pp. 852–863, 2012.
- [13] Y. Gao, H. Ao, Q. Zhou, Z. Feng, W. Zhou, Y. Li, and X. Li, "Modeling of Satellite Communication Systems Design with Physical Layer Security," in *2017 International Conference on Wireless Communications, Signal Processing and Networking (WiSPNET)*, 2017, pp. 1680–1683.
- [14] Y. Xiao, J. Liu, Y. Shen, X. Jiang, and N. Shiratori, "Secure Communication in Non-Geostationary Orbit Satellite Systems: A Physical Layer Security Perspective," *IEEE Access*, vol. 7, pp. 3371–3382, 2019.
- [15] K. Guo, K. An, B. Zhang, Y. Huang, X. Tang, G. Zheng, and T. A. Tsiftsis, "Physical Layer Security for Multiuser Satellite Communication Systems With Threshold-Based Scheduling Scheme," *IEEE Transactions on Vehicular Technology*, vol. 69, no. 5, pp. 5129–5141, 2020.
- [16] Y. Shi, J. Liu, J. Wang, and Y. Xun, "Jamming-aided Secure Communication in Ultra-dense LEO Integrated Satellite-Terrestrial Networks," *China Communications*, vol. 20, no. 7, pp. 43–56, 2023.

- [17] Z. Yin, M. Jia, N. Cheng, W. Wang, F. Lyu, Q. Guo, and X. Shen, "UAV-Assisted Physical Layer Security in Multi-Beam Satellite-Enabled Vehicle Communications," *IEEE Transactions on Intelligent Transportation Systems*, vol. 23, no. 3, pp. 2739–2751, 2022.
- [18] J. Bas and A. Perez-Neira, "On the Physical Layer Security of IoT Devices over Satellite," in *2019 27th European Signal Processing Conference (EUSIPCO)*, 2019, pp. 1–5.
- [19] Z. Lin, M. Lin, B. Champagne, W.-P. Zhu, and N. Al-Dhahir, "Secrecy-Energy Efficient Hybrid Beamforming for Satellite-Terrestrial Integrated Networks," *IEEE Transactions on Communications*, vol. 69, no. 9, pp. 6345–6360, 2021.
- [20] Z. Lin, K. An, H. Niu, Y. Hu, S. Chatzinotas, G. Zheng, and J. Wang, "SLNR-Based Secure Energy Efficient Beamforming in Multibeam Satellite Systems," *IEEE Transactions on Aerospace and Electronic Systems*, vol. 59, no. 2, pp. 2085–2088, 2023.
- [21] Z. Lin, H. Niu, K. An, Y. Wang, G. Zheng, S. Chatzinotas, and Y. Hu, "Refracting RIS-Aided Hybrid Satellite-Terrestrial Relay Networks: Joint Beamforming Design and Optimization," *IEEE Transactions on Aerospace and Electronic Systems*, vol. 58, no. 4, pp. 3717–3724, 2022.
- [22] Z. Lin, M. Lin, T. de Cola, J.-B. Wang, W.-P. Zhu, and J. Cheng, "Supporting IoT With Rate-Splitting Multiple Access in Satellite and Aerial-Integrated Networks," *IEEE Internet of Things Journal*, vol. 8, no. 14, pp. 11 123–11 134, 2021.
- [23] D.-H. Jung, J.-G. Ryu, W.-J. Byun, and J. Choi, "Performance Analysis of Satellite Communication System Under the Shadowed-Rician Fading: A Stochastic Geometry Approach," *IEEE Transactions on Communications*, vol. 70, no. 4, pp. 2707–2721, 2022.
- [24] A. Al-Hourani, "An Analytic Approach for Modeling the Coverage Performance of Dense Satellite Networks," *IEEE Wireless Communications Letters*, vol. 10, no. 4, pp. 897–901, 2021.
- [25] Z. Lou, B. E. Y. Belmekki, and M.-S. Alouini, "Coverage analysis of hybrid RF/THz networks with best relay selection," *IEEE Communications Letters*, vol. 27, no. 6, pp. 1634–1638, 2023.
- [26] M. Haenggi, *Stochastic Geometry for Wireless Networks*. Cambridge University Press, 2012.
- [27] R. Wang, M. A. Kishk, and M.-S. Alouini, "Reliability analysis of multi-hop routing in multi-tier LEO satellite networks," *IEEE Transactions on Wireless Communications*, Mar. 2024, early Access.
- [28] B. Al Homssi and A. Al-Hourani, "Optimal Beamwidth and Altitude for Maximal Uplink Coverage in Satellite Networks," *IEEE Wireless Communications Letters*, vol. 11, no. 4, pp. 771–775, April 2022.
- [29] A. Talgat, M. A. Kishk, and M.-S. Alouini, "Nearest Neighbor and Contact Distance Distribution for Binomial Point Process on Spherical Surfaces," *IEEE Communications Letters*, vol. 24, no. 12, pp. 2659–2663, 2020.
- [30] Z. Lou, B. E. Y. Belmekki, and M.-S. Alouini, "HAPS in the non-terrestrial network nexus: Prospective architectures and performance insights," *IEEE Wireless Communications*, vol. 30, no. 6, pp. 52–58, 2023.
- [31] R. Wang, M. A. Kishk, and M.-S. Alouini, "Evaluating the Accuracy of Stochastic Geometry Based Models for LEO Satellite Networks Analysis," *IEEE Communications Letters*, vol. 26, no. 10, pp. 2440–2444, 2022.
- [32] N. Okati, T. Riihonen, D. Korpi, I. Angervuori, and R. Wichman, "Downlink Coverage and Rate Analysis of Low Earth Orbit Satellite Constellations Using Stochastic Geometry," *IEEE Transactions on Communications*, vol. 68, no. 8, pp. 5120–5134, 2020.
- [33] R. Wang, M. A. Kishk, and M.-S. Alouini, "Ultra reliable low latency routing in LEO satellite constellations: A stochastic geometry approach," *IEEE Journal on Selected Areas in Communications*, 2024.
- [34] —, "Ultra-Dense LEO Satellite-Based Communication Systems: A Novel Modeling Technique," *IEEE Communications Magazine*, vol. 60, no. 4, pp. 25–31, 2022.
- [35] A. Talgat, M. A. Kishk, and M.-S. Alouini, "Stochastic Geometry-based Uplink Performance Analysis of IoT over LEO Satellite Communication," *IEEE Transactions on Aerospace and Electronic Systems*, 2024, Early Access.

- [36] D. Kim and N. Lee, "Ergodic Secrecy Rate Analysis for LEO Satellite Downlink Networks," 2023, [Online]. Available: <https://arxiv.org/abs/2312.06985>.
- [37] D.-H. Jung, J.-G. Ryu, and J. Choi, "When Satellites Work as Eavesdroppers," *IEEE Transactions on Information Forensics and Security*, vol. 17, pp. 2784–2799, 2022.
- [38] A. Talgat, M. A. Kishk, and M.-S. Alouini, "Stochastic Geometry-Based Analysis of LEO Satellite Communication Systems," *IEEE Communications Letters*, vol. 25, no. 8, pp. 2458–2462, 2021.
- [39] M. Kamel, W. Hamouda, and A. Youssef, "Physical Layer Security in Ultra-Dense Networks," *IEEE Wireless Communications Letters*, vol. 6, no. 5, pp. 690–693, 2017.
- [40] H. Chamkhia, A. Al-Ali, A. Mohamed, M. Guizani, A. Erbad, and A. Refaey, "Performance Analysis of IoT Physical Layer Security Using 3-D Stochastic Geometry," in *2020 International Conference on Computational Science and Computational Intelligence (CSCI)*, 2020, pp. 1022–1027.
- [41] H. Wang, X. Zhou, and M. C. Reed, "Physical Layer Security in Cellular Networks: A Stochastic Geometry Approach," *IEEE Transactions on Wireless Communications*, vol. 12, no. 6, pp. 2776–2787, 2013.
- [42] M. Ragheb, S. M. S. Hemami, A. Kuhestani, D. W. K. Ng, and L. Hanzo, "On the Physical Layer Security of Untrusted Millimeter Wave Relaying Networks: A Stochastic Geometry Approach," *IEEE Transactions on Information Forensics and Security*, vol. 17, pp. 53–68, 2022.
- [43] W. Wang, K. C. Teh, and K. H. Li, "Artificial Noise Aided Physical Layer Security in Multi-Antenna Small-Cell Networks," *IEEE Transactions on Information Forensics and Security*, vol. 12, no. 6, pp. 1470–1482, 2017.
- [44] C. Loo, "A Statistical Model for a Land Mobile Satellite Link," *IEEE Transactions on Vehicular Technology*, vol. 34, no. 3, pp. 122–127, 1985.
- [45] A. Abdi, W. C. Lau, M.-S. Alouini, and M. Kaveh, "A New Simple Model for Land Mobile Satellite Channels: First- and Second-Order Statistics," *IEEE Transactions on Wireless Communications*, vol. 2, no. 3, pp. 519–528, 2003.
- [46] R. Wang, M. A. Kishk, and M.-S. Alouini, "Stochastic Geometry-Based Low Latency Routing in Massive LEO Satellite Networks," *IEEE Transactions on Aerospace and Electronic Systems*, vol. 58, no. 5, pp. 3881–3894, 2022.